Structural Characterization of 4-Bromostyrene Self-Assembled Monolayers on Si(111)

Rajiv Basu, Jui-Ching Lin, Chang-Yong Kim, Matthew J. Schmitz, Nathan L. Yoder, Joshua A. Kellar, Michael J. Bedzyk, and Mark C. Hersam*

Department of Materials Science and Engineering, Northwestern University, Evanston, Illinois 60208-3108

Received September 20, 2006. In Final Form: November 14, 2006

Organic functionalization of silicon holds promise for a variety of applications ranging from molecular electronics to biosensing. Because the performance and reliability of organosilicon devices will be intimately tied to the detailed structure of the organic adlayers, it is imperative to develop systematic strategies for forming and characterizing self-assembled monolayers (SAMs) on silicon with submolecular spatial resolution. In this study, we use 4-bromostyrene for the photochemical growth of Br-terminated SAMs on Si(111). A variety of experimental and theoretical techniques including atomic force microscopy (AFM), X-ray photoelectron spectroscopy (XPS), X-ray reflectivity (XRR), X-ray standing waves (XSW), X-ray fluorescence (XRF), and density functional theory (DFT) have been employed to determine the coverage and conformation of the 4-bromostryene molecules within the SAM. In particular, AFM verifies a continuous and atomically flat SAM, and the XRR data indicate a SAM thickness of 8.50 Å and a molecular coverage of 46% of the surface silicon atoms. Because the DFT calculations indicate a molecular length of 8.89 Å, the measured XRR thickness implies a molecular tilt angle of approximately 17°. The XRR analysis also suggests that the Br atoms are preserved on top of the SAM in agreement with XPS measurements that show bromine bound solely to carbon and not to silicon. XRF reveals a Br atomic coverage of 50%, again in close agreement to that found by XRR. Single-crystal Bragg diffraction XSW is used to generate a three-dimensional map of the Br distribution within the SAM, which in conjunction with the XRR result suggests that the 4-bromostyrene molecules are tilted such that the Br atoms are located over the T_4 sites at a height of 8.50 Å above the top bulklike Si(111) layer. The direction of molecular tilt toward the T_4 sites is consistent with that predicted by the DFT calculation. Overall, through this unique suite of complementary structural characterization techniques, it is concluded that the Br functional handle is preserved at the top of the SAM and is available for further substitutional chemistry.

1. Introduction

Since the seminal papers by Linford and Chidsey,[1,2] organic functionalization of silicon substrates has garnered significant attention from the scientific community.[3] For sensing applications, ordered self-assembled monolayers (SAMs) with terminal functionalities designed to react selectively with target analytes have been pursued.[4−11] In addition, the discrete molecular orbital energy levels of the organic terminations can couple with the band gap of the underlying semiconducting substrate to enable nonlinear charge transport in hybrid organosilicon devices.[12−25] The general approach for creating SAMs on silicon substrates has been through hydrosilylation of 1-alkenes by catalytic,[2] thermal,[26] and photoinduced[27] reactions.

Rather than developing monolayer chemistries for a desired functionality, emphasis has been placed on a more general approach of creating SAMs with terminal moieties that can then enable a variety of desired subsequent functionalizations. In this regard, the most prevalent approach has been the use of 1-alkenes

* Corresponding author. E-mail: m-hersam@northwestern.edu. WWW: http://www.hersam-group.northwestern.edu/. Tel: (847) 491-2696. Fax: (847) 491-7820.

(1) Linford, M. R.; Chidsey, C. E. D. *J. Am. Chem. Soc.* **1993**, *115*, 12631−12632.
(2) Linford, M. R.; Fenter, P.; Eisenberger, P. M.; Chidsey, C. E. D. *J. Am. Chem. Soc.* **1995**, *117*, 3145−3155.
(3) Buriak, J. M. *Chem. Rev.* **2002**, *102*, 1271−1308.
(4) Strother, T.; Cai, W.; Zhao, X. S.; Hamers, R. J.; Smith, L. M. *J. Am. Chem. Soc.* **2000**, *122*, 1205−1209.
(5) Lin, Z.; Strother, T.; Cai, W.; Cao, X. P.; Smith, L. M.; Hamers, R. J. *Langmuir* **2002**, *18*, 788−796.
(6) Wagner, P.; Nock, S.; Spudich, J. A.; Volkmuth, W. D.; Chu, S.; Cicero, R. L.; Wade, C. P.; Linford, M. R.; Chidsey, C. E. D. *J. Struct. Biol.* **1997**, *119*, 189−201.
(7) Wei, F.; Sun, B.; Guo, Y.; Zhao, X. S. *Biosens. Bioelectron.* **2003**, *18*, 1157−1163.
(8) Ivanisevic, A.; Mirkin, C. A. *J. Am. Chem. Soc.* **2001**, *123*, 7887−7889.
(9) Langner, A.; Panarello, A.; Rivillon, S.; Vassylyev, O.; Khinast, J. G.; Chabal, Y. J. *J. Am. Chem. Soc.* **2005**, *127*, 12798−12799.
(10) Perring, M.; Dutta, S.; Arafat, S.; Mitchell, M.; Kenis, P. J. A.; Bowden, N. B. *Langmuir* **2005**, *21*, 10537−10544.
(11) Allongue, P.; de Villeneuve, C. H.; Pinson, J.; Ozanam, F.; Chazalviel, J. N.; Wallart, X. *Electrochim. Acta* **1998**, *43*, 2791−2798.
(12) Guisinger, N. P.; Greene, M. E.; Basu, R.; Baluch, A. S.; Hersam, M. C. *Nano Lett.* **2004**, *4*, 55−59.
(13) Rakshit, T.; Liang, G. C.; Ghosh, A. W.; Datta, S. *Nano Lett.* **2004**, *4*, 1803−1807.
(14) Rakshit, T.; Liang, G. C.; Ghosh, A. W.; Hersam, M. C.; Datta, S. *Phys. Rev. B* **2005**, *72*, 125305.
(15) Guisinger, N. P.; Yoder, N. L.; Hersam, M. C. *Proc. Natl. Acad. Sci. U.S.A.* **2005**, *102*, 8838−8843.
(16) Basu, R.; Guisinger, N. P.; Greene, M. E.; Hersam, M. C. *Appl. Phys. Lett.* **2004**, *85*, 2619−2621.
(17) Hersam, M. C.; Reifenberger, R. G. *MRS Bull.* **2004**, *29*, 385−390.
(18) Guisinger, N. P.; Basu, R.; Greene, M. E.; Baluch, A. S.; Hersam, M. C. *Nanotechnology* **2004**, *15*, S452−S458.
(19) Guisinger, N. P.; Basu, R.; Baluch, A. S.; Hersam, M. C. *Ann. N.Y. Acad. Sci.* **2003**, *1006*, 227−234.
(20) Beckman, R.; Beverly, K.; Boukai, A.; Bunimovich, Y.; Choi, J. W.; DeIonno, E.; Green, J.; Johnston-Halperin, E.; Luo, Y.; Sheriff, B.; Stoddart, J. F.; Heath, J. R. *Faraday Discuss.* **2006**, *131*, 9−22.
(21) Blum, A. S.; Kushmerick, J. G.; Long, D. P.; Patterson, C. H.; Yang, J. C.; Henderson, J. C.; Yao, Y. X.; Tour, J. M.; Shashidhar, R.; Ratna, B. R. *Nat. Mater.* **2005**, *4*, 167−172.
(22) Gowda, S.; Mathur, G.; Li, Q. L.; Surthi, S.; Misra, V. *IEEE Trans. Nanotechnol.* **2006**, *5*, 258−264.
(23) Teplyakov, A. V.; Kong, M. J.; Bent, S. F. *J. Am. Chem. Soc.* **1997**, *119*, 11100−11101.
(24) Lenfant, S.; Krzeminski, C.; Delerue, C.; Allan, G.; Vuillaume, D. *Nano Lett.* **2003**, *3*, 741−746.
(25) Piva, P. G.; DiLabio, G. A.; Pitters, J. L.; Zikovsky, J.; Rezeq, M.; Dogel, S.; Hofer, W. A.; Wolkow, R. A. *Nature* **2005**, *435*, 658−661.
(26) Sieval, A. B.; Demirel, A. L.; Nissink, J. W. M.; Linford, M. R.; van der Maas, J. H.; de Jeu, W. H.; Zuilhof, H.; Sudholter, E. J. R. *Langmuir* **1998**, *14*, 1759−1768.
(27) Cicero, R. L.; Linford, M. R.; Chidsey, C. E. D. *Langmuir* **2000**, *16*, 5688−5695.

10.1021/la062759f CCC: $37.00
Published on Web 01/06/2007

with ω functionalities, including ester[4,26,28] and amine[5,29,30] moieties. However, being reactive entities themselves, these terminal moieties can also undergo undesired attachment to the silicon substrate. To avoid this possibility, the terminal moiety can be protected during SAM formation and then subsequently deprotected to make it available for further chemistry.[5,26] However, following SAM formation, steric hindrance imposed by neighboring molecules in the SAM limits accessibility by the deprotecting agents, thus decreasing the effectiveness of the protection−deprotection cycle. Furthermore, the added bulkiness of the protective groups can limit the ordering and coverage of the SAM.

Consequently, because of these limitations, it is desirable to identify a molecular system that allows the formation of dense silicon-based SAMs with a functional terminal moiety that does not require any additional chemical protection. Here, the underlying philosophy is the judicious choice of a SAM-forming organic molecule that inherently preserves its ω functionality without further need of an external protecting agent. Coherent with this vision, in a recent paper, we identified 4-bromostyrene (**Br-Sty**) as a suitable candidate molecule for growing dense SAMs with intact Br atom termination that offers the chemical handle to perform further substitution chemistry on top of the monolayer.[31] Previously, we had reported that similar attempts to grow Br-terminated SAMs using undec-10-enoic acid 2-bromoethyl ester (**Br-UDAME**) had resulted in the loss of Br atoms to the silicon radicals.[32] These two results led us to conclude that the tendency toward Br abstraction by the surface silicon is governed by the stability of the resultant organic radical.[31] Thus, the relative instability of the phenyl radical that would form if Br were abstracted from **Br-Sty** is attributed to the successful preservation of the halogen termination of the corresponding SAM.

This article is a continuation of our studies of Br-terminated adlayers on silicon and is motivated by the need to elucidate the physical structure of a terminally functionalized SAM. A detailed characterization of various structural parameters (e.g., thickness, packing density, and molecular tilt) will help us to design the subsequent chemical reaction for the next layer of functionalization so that the steric hindrance of the terminal moieties can be minimized. To achieve this objective, we employed a variety of surface-sensitive experimental techniques. Atomic force microscopy (AFM) was utilized for surface morphology verification, and X-ray photoelectron spectroscopy (XPS) allowed chemical bonding within the SAM to be characterized. As an X-ray fluorescent tag, Br offers the option of physical interrogation by a variety of additional complimentary X-ray-based techniques. For example, the monolayer thickness, molecular tilt, packing density, and interface roughness were interrogated using X-ray reflectivity (XRR). The packing density was also independently confirmed by X-ray fluorescence (XRF). Finally, single-crystal X-ray standing wave (XSW) data were used to generate a three-dimensional map of the Br distribution within the SAM and to triangulate the position of the Br atoms with respect to the underlying Si(111) lattice. These experimental observations were then directly compared with density functional theory (DFT) calculations. The unique combination of these techniques provides a thorough characterization of silicon-based SAMs with sub-molecular spatial resolution.

2. Experimental Section

Preparation of Hydrogen-Passivated Si(111) Substrates. Hydrogen passivation of the silicon surfaces was achieved by following the procedure described by Higashi et al.[33] Samples were cut from single-side-polished silicon (111) wafers (Virginia Semiconductors, 0.25° miscut in the $\langle 110 \rangle \pm 0.1°$ direction, phosphorus-doped, resistivity = 0.05−0.07 Ω·cm). Prior to passivation, each sample was rinsed with acetone and methanol. Initial passivation was accomplished by submerging the samples in a 0.5% solution of HF for 30 s. They were then submerged in argon-sparged ultrapure 18 MΩ·cm water for 5 s. To remove organic contaminants, the samples were next immersed in a solution of 4:1 (v/v) H_2SO_4/30% H_2O_2(aq) for 10 min at 90 °C. Following this treatment, the samples were again submerged in argon-sparged 18 MΩ·cm water for 5 s. To create an atomically flat terraced surface, the samples were subsequently immersed in argon-sparged, clean-room-grade 40% NH_4F(aq) for 30 min. During this time, the tube used for argon sparging was held over the NH_4F solution to minimize the amount of oxygen that could dissolve into the solution and cause surface pitting. A final 1 min immersion in argon-sparged 18 MΩ·cm water was performed, following which the samples were blown dry with a N_2 gun and stored in an inert atmosphere glove box (Nexus, Vacuum Atmospheres) maintained at a slightly positive N_2 pressure (99.999% purity, <1.5 ppm O_2, <0.5 ppm H_2O). The purpose of this final rinse was to minimize the number of residual fluorine atoms on the silicon surface and in turn decrease the rate of adsorption of organic contaminants on the surface.[34] The passivated samples were stored in the glove box until subsequent SAM growth and surface analysis.

Preparation of a 4-Bromostyrene SAM on Si(111). A 254 nm pen lamp was used to grow **Br-Sty** SAMs photochemically on the hydrogen-terminated Si(111) surface inside the inert atmosphere glove box. Neat **Br-Sty** (Sigma-Aldrich, 98%) was pipetted to form a thin layer covering the entire surface. Monolayer growth was achieved by irradiating this reagent-covered surface with the pen lamp from a distance of 1 cm for about 2.5 h. The samples were then brought out of the glove box for 10 min rinses in toluene and chloroform and then returned to the glove box for storage until further analysis.

Atomic Force Microscopy. AFM images were taken on the Si(111) surfaces following hydrogen passivation, as well as following the subsequent growth of the **Br-Sty** SAM. Imaging was done with an Autoprobe CP Research AFM using triangular silicon ultralevers with 2.0−5.1 N/m spring constants. The images were taken in contact mode under ambient air conditions at approximately 20% relative humidity and 25 °C.

X-ray Photoelectron Spectroscopy. XPS analysis was performed at the Keck Interdisciplinary Surface Science Center of Northwestern University using an Omicron ESCA probe. A monochromated Al Kα beam radiating at 1486.6 eV was incident on the sample surface that was oriented such that the emitted photoelectrons had a takeoff angle of 45° from the sample surface to the analyzer. A survey scan was initially performed with a pass energy of 500 meV to verify the presence of Br on the surface following SAM formation. Subsequently, high-resolution Br 3d spectra were obtained by sweeping over the appropriate energy range eight times using an analyzer pass energy of 25 meV. The energy position of the spectra was referenced with respect to that of the adventitious C 1s peak fixed at 284.8 eV.

Density Functional Theory. A $Si_{26}H_{30}$ silicon cluster was chosen to approximate the silicon surface in the vicinity of the adsorption site of the **Br-Sty** molecule as well as three layers of the underlying silicon substrate. A **Br-Sty** molecule was bonded to the central silicon atom in the top layer, and all other silicon atoms were passivated with hydrogen. The cluster was constructed using HyperChem

(28) Boukherroub, R.; Wayner, D. D. M. *J. Am. Chem. Soc.* **1999**, *121*, 11513−11515.
(29) Strother, T.; Hamers, R. J.; Smith, L. M. *Nucleic Acids Res.* **2000**, *28*, 3535−3541.
(30) Sieval, A. B.; Linke, R.; Heij, G.; Meijer, G.; Zuilhof, H.; Sudholter, E. J. R. *Langmuir* **2001**, *17*, 7554−7559.
(31) Basu, R.; Kinser, C. R.; Tovar, J. D.; Hersam, M. C. *Chem. Phys.* **2006**, *326*, 144−150.
(32) Jin, H.; Kinser, C. R.; Bertin, P. A.; Kramer, D. E.; Libera, J. A.; Hersam, M. C.; Nguyen, S. T.; Bedzyk, M. J. *Langmuir* **2004**, *20*, 6252−6258.
(33) Higashi, G. S.; Chabal, Y. J.; Trucks, G. W.; Raghavachari, K. *Appl. Phys. Lett.* **1990**, *56*, 656−658.
(34) Saga, K.; Hattori, T. *J. Electrochem. Soc.* **1997**, *144*, L250−L252.

Release 7 (Hypercube, Inc., Gainesville, FL) and optimized using molecular mechanics. The cluster was further optimized using DFT within the Q-Chem electronic structure package.[35] The B3LYP density functional[36] was chosen to account for electron exchange and correlation effects, and a 6-31G* all-electron basis set[37,38] with polarization functions was employed for all atoms. The cluster was allowed to optimize its geometry without constraint. The β carbon radical of the **Br-Sty** was capped with hydrogen to mimic the structure of a single molecule following abstraction of a hydrogen from the H−Si(111) surface. Similar models were used by Pei and Ma[39,40] to study the behavior of octadecanal, octadecene, and styrene molecules on the H−Si(111) surface. From the equilibrium structure, the height of the Br atom above the silicon surface can be calculated and compared with the experimental XRR and XSW data.

X-ray Reflectivity. Specular XRR measurements were performed on a Rigaku ATX-G rotating anode four-circle diffractometer at the Northwestern University X-ray Facility with Cu Kα radiation (λ = 1.542 Å) operating at 50 kV and 240 mA. The incident beam was conditioned by a multilayer parabolic collimating mirror, followed by a 0.1-mm-wide × 5-mm-high incident beam slit. The incident photon flux was 2×10^8 photons/s. The instrumental resolution for the perpendicular wave-vector transfer $Q = (4\pi \sin\theta)/\lambda$ was $\Delta Q = 5 \times 10^{-3}$ Å^{-1}. The reflectivity data was background subtracted, dead time corrected, and normalized to the straight-through beam intensity.

X-ray Standing Wave and Fluorescence. The Br atomic distribution relative to the Si lattice was studied by XSW measurements, performed at the Advanced Photon Source (APS) 5ID-C undulator station. The 5ID-C experimental setup is more fully described elsewhere.[41] The XSW measurements consist of simultaneously monitoring the reflectivity and XRF while scanning the angle through an $H = hkl$ bulk Bragg peak.[42−44]

The incident photon energy was tuned by the undulator third harmonic and by the high-heat-load Si(111) monochromator to 15.05 keV to excite Br Kα fluorescence. XSW data was collected for the Si(111), (333), (11$\bar{1}$), and (220) Bragg reflections. A two-bounce Si(111) or (333) or (220) channel-cut post-monochromator crystal was used to create a nondispersive reflection from the sample. For the Si(111) measurement, the incident beam slit was 0.2 mm high × 1 mm wide, and the incident beam flux was 1.3×10^{11} photons/s. XRF spectra were collected with a germanium solid-state detector and corrected for dead time. The normalized Br fluorescence yield is given by

$$Y(\theta) = 1 + R(\theta) + 2\sqrt{R(\theta)}\, f_H \cos[\nu(\theta) - 2\pi P_H] \qquad (1)$$

where the reflectivity (R) and XSW phase (ν) are derived from dynamical diffraction theory.[42,44] We determine the coherent fraction, f_H, and coherent position, P_H, by a χ^2 fit of eq 1 to the data. The combination of specular and off-specular XSW measurements is used to three-dimensionally triangulate the Br site relative to the Si lattice.[43] Because f_H and P_H are the *hkl* Fourier amplitude and phase, respectively, of the Br atomic distribution, we are able to generate

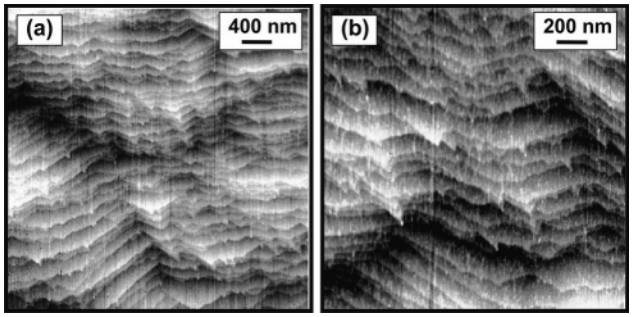

Figure 1. AFM topography images of Si(111) surfaces following (a) wet-chemical hydrogen passivation and (b) subsequent growth of a 4-bromostyrene SAM. The similarities in morphology and step height for the two images indicate the formation of a dense monolayer of 4-bromostyrene on the latter surface.

a model-independent Br atomic 3D map by the following Fourier inversion:[45−47]

$$\rho(\mathbf{r}) = \sum_H f_H \exp[2\pi i(P_H - \mathbf{H}\cdot\mathbf{r})] = 1 + 2\sum_{\substack{H \neq -H \\ H \neq 0}} f_H \cos[2\pi(P_H - \mathbf{H}\cdot\mathbf{r})] \qquad (2)$$

A review of the theory underlying this type of XSW analysis is described elsewhere.[42]

The Br coverage of each sample was measured by comparing the Br Kα XRF yield to the As Kβ yield from an As implanted standard with an As coverage calibrated by Rutherford backscattering. At 15.05 keV, the Br Kα to As Kβ XRF cross-sectional ratio is 8.41. A 1 monolayer (ML) coverage corresponds to 7.83 atoms/nm^2. This number is the atomic density of the topmost Si atomic layer in the 1 × 1 Si(111) bulklike surface.

For all X-ray experiments, the samples were sealed within a dry-nitrogen flow cell with a thin Kapton X-ray window to avoid air exposure and oxidation. X-ray radiation damage effects were closely monitored and minimized during exposure to the monochromatic undulator beam. This was done by using incident beam transmission filters and a fast shutter and by moving the footprint of the beam on the sample to a fresh unradiated spot before any significant damage occurred. Under the full undulator intensity of 1×10^{11} photons/s per mm^2 of radiated surface area, the Br coverage showed an X-ray-induced desorption effect corresponding to an exponential decay with a half-life of 10 min.

3. Results and Discussion

AFM imaging of the surface following photochemical attachment of **Br-Sty** indicates the formation of a densely packed SAM on Si(111). Figure 1a shows an AFM image of a typical wet-chemical-passivated H−Si(111) surface with a step height of 3.1 Å. Figure 1b shows an AFM image of the Si(111) surface following the growth of the **Br-Sty** monolayer. These topographic images show that the step height and morphology are preserved before and after SAM growth and are thus indicative of the formation of a dense monolayer.[6] Additionally, consistent with the formation of 1D molecular chains of **Br-Sty** on the monohydride H−Si(100)-2 × 1 surface,[31] the monolayer imaged in Figure 1b is likely to be made of islands of **Br-Sty** chains formed by a self-avoiding, near-random-walk radical chain

(35) Kong, J.; White, C. A.; Krylov, A. I.; Sherrill, D.; Adamson, R. D.; Furlani, T. R.; Lee, M. S.; Lee, A. M.; Gwaltney, S. R.; Adams, T. R.; Ochsenfeld, C.; Gilbert, A. T. B.; Kedziora, G. S.; Rassolov, V. A.; Maurice, D. R.; Nair, N.; Shao, Y. H.; Besley, N. A.; Maslen, P. E.; Dombroski, J. P.; Daschel, H.; Zhang, W. M.; Korambath, P. P.; Baker, J.; Byrd, E. F. C.; Van, Voorhis, T.; Oumi, M.; Hirata, S.; Hsu, C. P.; Ishikawa, N.; Florian, J.; Warshel, A.; Johnson, B. G.; Gill, P. M. W.; Head-Gordon, M.; Pople, J. A. *J. Comput. Chem.* **2000**, *21*, 1532−1548.

(36) Becke, A. D. *J. Chem. Phys.* **1993**, *98*, 5648−5652.

(37) Harihara, Pc.; Pople, J. A. *Theor. Chim. Acta* **1973**, *28*, 213−222.

(38) Francl, M. M.; Pietro, W. J.; Hehre, W. J.; Binkley, J. S.; Gordon, M. S.; Defrees, D. J.; Pople, J. A. *J. Chem. Phys.* **1982**, *77*, 3654−3665.

(39) Pei, Y.; Ma, J.; Jiang, Y. S. *Langmuir* **2003**, *19*, 7652−7661.

(40) Pei, Y.; Ma, J. *Langmuir* **2006**, *22*, 3040−3048.

(41) Walko, D. A.; Sakata, O.; Lyman, P. F.; Lee, T.-L.; Tinkham, B. P.; Okasinski, J. S.; Zhang, Z.; Bedzyk, M. J. *AIP Conf. Proc.* **2004**, *705*, 1166.

(42) For a review of XSW see: Bedzyk, M. J.; Cheng, L. W. *Rev. Mineral. Geochem.* **2002**, *49*, 221−266.

(43) Golovchenko, J. A.; Patel, J. R.; Kaplan, D. R.; Cowan, P. L.; Bedzyk, M. J. *Phys. Rev. Lett.* **1982**, *49*, 560−563.

(44) Zegenhagen, J. *Surf. Sci. Rep.* **1993**, *18*, 199−271.

(45) Bedzyk, M. J.; Fenter, P.; Zhang, Z.; Cheng, L.; Okasinski, J. S.; Sturchio, N. C. *Synchrotron Radiat. News (Tech. Rev.)* **2004**, *17*, 5−10.

(46) Cheng, L.; Fenter, P.; Bedzyk, M. J.; Sturchio, N. C. *Phys. Rev. Lett.* **2003**, *90*, 255503.

(47) Okasinski, J. S.; Kim, C.; Walko, D. A.; Bedzyk, M. J. *Phys. Rev. B* **2004**, *69*, 041401.

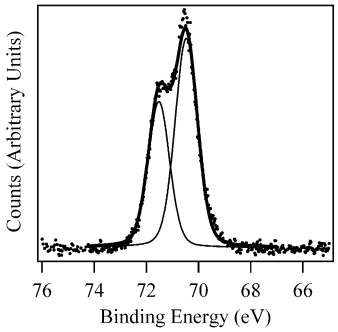

Figure 2. High-resolution XPS spectrum obtained from a 4-bromostyrene SAM on the Si(111) surface. This spectrum shows a single Br 3d spin doublet at 70.5 and 71.5 eV, which is attributed to carbon-bound bromine.

mechanism analogous to that observed for 1-decene on the H−Si(111) surface.[48]

The chemical bonding state of the SAM was confirmed by XPS analysis of the **Br-Sty** monolayer. Using the XPSPeak 4.1 program,[49] high-resolution Br 3d spectra obtained from the monolayer were fitted with Gaussian−Lorentzian sum functions. Consistent with the Br 3d spin doublet, the fitted pairs of curves were subjected to the constraint of $\Delta E = 1.05$ eV and a peak area ratio of 2:3.[50] As shown in Figure 2, the best fit for the Br 3d XPS spectrum was obtained using only a single pair of peaks, indicating the existence of bromine in only one oxidation state. Specifically, this state is attributed to carbon-bound bromine because the Br 3d spin doublet is positioned at 70.5 and 71.5 eV[31,32,51] and confirms the presence of bromophenyl groups on the surface following monolayer formation.[52,53] Thus, XPS analysis of the surface further supports the premise that the monolayer is composed of **Br-Sty** molecular chains formed by a surface radical propagating chain mechanism,[27] whereby the Br atoms remain attached to their respective phenyl rings and form the topmost part of the organic adlayer.

DFT calculations were performed to determine the thickness of the **Br-Sty** monolayer. Parts a and b of Figure 3 show the front and top views, respectively, of a **Br-Sty** molecule tethered to a T_1 Si atom of a $Si_{26}H_{30}$ silicon cluster following unconstrained geometry optimization. The molecular length of **Br-Sty** is calculated as the distance between the centers of the Br atom and the Si atom under the T_1 site and is found to be 8.89 Å. The SAM thickness, t, is determined as the height of the bromine atom with respect to the T_1 Si atom ($t = z_{Br} - z_{Si,T_1}$). The molecular length and the SAM thickness are shown as dotted and solid red lines, respectively, in Figure 3a. For the equilibrium structure shown in Figure 3, $t = 8.86$ Å. This corresponds to a molecular tilt angle of $\eta = 5°$ (about the [111] axis at the T_1 site) and tilted in the direction of one of the three equivalent nearest Si T_4 sites. It should be noted that this DFT calculation employs only one **Br-Sty** molecule and hence does not take into account the intermolecular interactions that are likely to occur in a densely packed monolayer. Although these interactions should not change the molecular length, they could certainly influence the structure

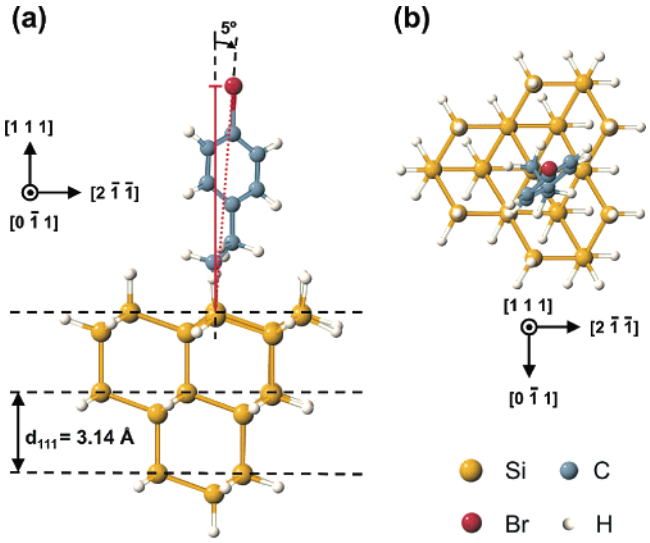

Figure 3. DFT optimized 4-bromostyrene−$Si_{26}H_{30}$ cluster model used to determine the height of the Br atom and the molecular tilt: (a) side view and (b) top view. The silicon atoms have been terminated with hydrogen, and the β carbon of 4-bromostyrene is capped with hydrogen to mimic the structure of a molecule following hydrogen abstraction during the radical propagation growth mechanism. The optimized structure has a molecular tilt angle of $\eta = 5°$ about the [111] axis at the T_1 site. The silicon d_{111} spacing in panel a is 3.14 Å.

of the SAM, including the tilt angle and hence the thickness, t. Consequently, these DFT calculations are aimed at finding the molecular length as well as an initial estimation of the monolayer thickness, which will be used as starting parameters for fitting the X-ray data.

The XRR measurement of this SAM sample is sensitive to the gradient in the electron density profile $\rho'(z)$.[54] As such, it will be sensitive to the molecular packing density, film thickness, interface roughness, and height/location of the Br layer relative to the Si/SAM interface. The XRR data in Figure 4 is compared to six different model calculations that are based on kinematic scattering theory for the specular rod intensity that occurs between the 000 and 111 Si Bragg peaks.[55] Referring to the DFT-calculated structure shown in Figure 3, the **Br-Sty** molecule in these reflectivity calculations is accounted for by a 1D structure factor, $F(Q)$, that is determined from the z coordinates of the non-hydrogen atoms. In our modeling, the film thickness (t) is allowed to vary by changing the tilt angle (η) to the molecule about the T_1 Si site from its nominal DFT-determined configuration. The DFT-predicted film thickness (with $\eta = 5°$) is $t = 8.9$ Å. The best-fit curve to the data is labeled A1, which has (1) the molecule tilted further inward to $\eta = 17°$ (corresponding to $t = 8.5$ Å), (2) the molecular packing at a coverage of $\Theta = 0.46$ ML, (3) a static Gaussian vertical displacement distribution for all atoms in the molecule characterized by a width $\sigma = 1.0$ Å, and (4) the interface roughness parameter[55] at $\beta = 0.47$.

In Figure 4, the XRR sensitivity to molecular packing density is demonstrated by the accompanying curves labeled A2 and A3, where the coverage has been changed to 0.52 and 0.40 ML, respectively. As can be seen, the strength of the antireflection dip at $Q = 0.32$ Å^{-1} changes with coverage. Curves B1 and B2 illustrate the sensitivity to changing the film thickness by changing the molecular tilt angle to 5 and 53°, respectively. Curve B1 corresponds to the DFT model shown in Figure 3 ($t = 8.9$ Å), and curve B2 corresponds to $t = 5.3$ Å. The shift in Q of the

(48) Eves, B. J.; Sun, Q. Y.; Lopinski, G. P.; Zuilhof, H. *J. Am. Chem. Soc.* **2004**, *126*, 14318−14319.
(49) Kwok, R. W. M. Computer code *XPSPeak*, version 4.1; The Chinese University of Hong Kong: Shatin, New Territories, Hong Kong SAR, 1999.
(50) *Handbook of X-ray Photoelectron Spectroscopy*; Chastain, J., Ed.; Perkin-Elmer Corp., Physical Electronics Division: Eden Prairie, MN, 1995; Chapter 1, p 10; Chapter 2, p 98.
(51) Zhou, X. J.; Li, Q.; He, Z. H.; Yang, X.; Leung, K. T. *Surf. Sci.* **2003**, *543*, L668−L674.
(52) Deluge, M.; Cai, C. Z. *Langmuir* **2005**, *21*, 1917−1922.
(53) Beamson, G.; Briggs, D. *High Resolution XPS of Organic Polymers: The Scienta ESCA300 Database*. Wiley-Interscience: New York, 1992.
(54) Als-Nielsen, J.; McMorrow, D. *Elements of Modern X-ray Physics*; Wiley: New York, 2001.
(55) Robinson, I. K.; Tweet, D. J. *Rep. Prog. Phys.* **1992**, *55*, 599−651.

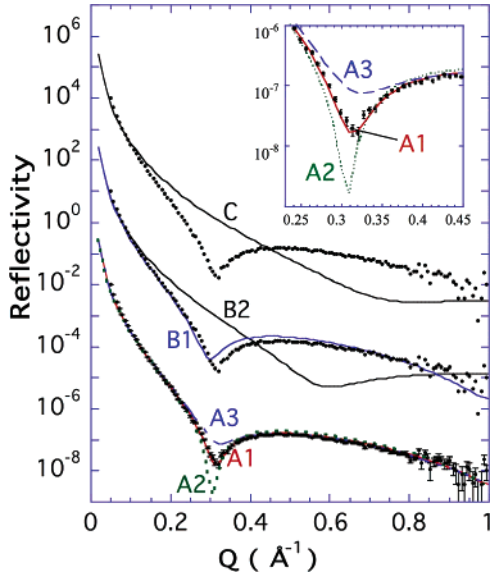

Figure 4. Specular XRR data (filled circles) and model simulations using a molecule structure factor with atomic coordinates based on the DFT calculation of Figure 3. The best-fit simulation is labeled A1. The A1 model has a molecular coverage of $\Theta = 0.46$ ML, an inward molecular tilt of $\eta = 17°$ ($t = 8.5$ Å), a Si surface roughness parameter of $\beta = 0.47$, and a $\sigma = 1.0$ Å Gaussian distribution of the vertical displacements of the atoms in the molecule. Model A2: same as A1 except that $\Theta = 0.52$ ML. A3: same as A1 except that $\Theta = 0.40$ ML. B1: same as A1 except that $\eta = 5°$ tilt ($t = 8.9$ Å). B2: same as A1 except that $\eta = 53°$ tilt ($t = 5.3$ Å). C: same as A1 except that Br is removed from styrene and attached directly to Si at the T_1 site. For purposes of clarity, the vertical offsets are $\times 10^3$ for B1 and B2 and $\times 10^6$ for C.

dip is quite sensitive to the height of the Br layer. (All other parameters in models A2, A3, B1, and B2 are identical to those described above for model A1.)

In our earlier study of the **Br-UDAME**/Si(111) SAM system, we discovered by XSW, XRR, and XPS that most of the Br dissociated from the molecules and covalently attached to the Si dangling bonds.[32] If this had occurred for the present **Br-Sty** case, then the XRR data would have followed the curve labeled C in Figure 4. The model for C is identical to that for A1, but with the Br detached from the styrene and attached to the remaining half monolayer of Si dangling bond sites with a Si−Br bond length of 2.2 Å. Note that curve C is missing a dip in this recorded Q range because of the missing fluctuation in $\rho'(z)$ at the top of the film.

The XRF-calibrated Br atomic coverage was determined to be $\Theta_{Br} \equiv 0.50$ ML. This measurement is in close agreement with the previously described XRR measured coverage of the **Br-Sty** molecules made independently on the same sample.

The XSW results listed in Table 1 are the average values obtained from several identically prepared samples. Because of desorption caused by X-ray dosage and exposure to air, the Br coverage for individual samples varied from 0.2 to 0.5 ML. However, the XSW-measured coherent position (P_H) and coherent fraction (f_H) values as listed in Table 1 were reproducible to within the listed uncertainties. The (111) XSW data and theoretical fit from eq 1 are shown in Figure 5. The origin for all of the coherent positions in our analysis is chosen to be the bulklike Si position in the top of the Si bilayer.

Using eq 2, the XSW-measured Fourier components listed in Table 1 (and their 3-fold symmetry equivalents) are summed to produce a Br 3D atomic density map with 2D cuts shown in Figure 6. Because this map is produced by allowed Si reflections,

Table 1. XSW Measured Values for the Br Coherent Fractions (f_H) and Coherent Positions (P_H)[a]

	measured values		DFT		modified DFT	
hkl	f_H	P_H	a_H	P_H	a_H	P_H
111	0.35(2)	0.71(1)	1.00	0.83	1.00	0.71
33$\bar{3}$	0.08(2)	0.10(6)	1.00	0.48	1.00	0.14
11$\bar{1}$	0.25(2)	0.35(2)	0.57	0.97	0.87	0.24
220	0.11(2)	1.00(3)	0.57	0.80	0.87	0.95

[a] Also listed are the model calculated values for the geometrical factor (a_H) and P_H for the Br distribution as predicted by the DFT model shown in Figure 3 with 3-fold symmetry creating three equally occupied lateral positions. The same information is listed for the modified DFT model depicted in Figure 7, where the 4-bromostyrene has been tilted to 17° to match the XSW P_{111} and XRR measured Br height.

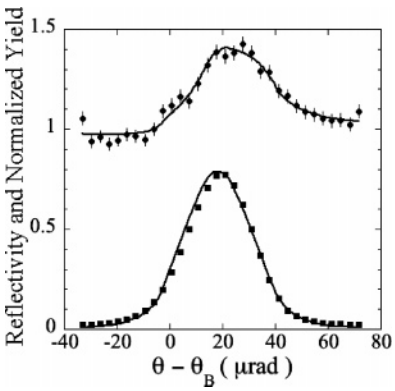

Figure 5. Single-crystal 111 XSW results for the 4-bromostyrene SAM on Si(111). Shown are the angle dependence of the Si(111) Bragg reflectivity "rocking curve" and the Br Kα XRF yield data. Symbols are measured data, and solid lines are the best fits of theory (including eq 1) to the data. The f_{111} and P_{111} parameters determined by this fit are listed in Table 1.

it has the same periodicity as the Si primitive unit cell (rhombohedral). Because this is the diamond-cubic 111 surface, we use a hexagonal unit cell for convenience. Equivalent maxima in the Br atomic density map show up at three symmetry-equivalent positions within this hexagonal unit cell. (Note that the volume of the hexagonal unit cell is 3 times that of the rhombohedral.) A Br maximum shows up above the 1-fold-coordinated top T_1 site at $z = P_{111}{*}d_{111} = 2.23$ Å, the 3-fold-coordinated hollow H_3 site at $z = (1 + P_{111})d_{111} = 5.37$ Å, and the 4-fold-coordinated top T_4 site at $z = (2 + P_{111})d_{111} = 8.50$ Å. The XSW measurement by itself cannot discriminate among these three possibilities. However, the XRR measurement and analysis in Figure 4 clearly indicate that Br is at $z = 8.5$ Å (curve A1) and not at the other two heights (curves B2 and C). The subsidiary maxima are due to the truncation of the Fourier summation (missing terms in the infinite sum). In addition to finding the Br height, we now also know that the correct maximum in the Br atomic density map is centered laterally above the T_4 site. Referring to Figure 7, this is consistent with the inward tilt of the **Br-Sty** molecule about the T_1 site combined with the 3-fold symmetry (about the [111] axis at the T_1 site) of the bulk-terminated Si(111) surface that will cause Br to equally occupy three chemically equivalent domains with generalized Br coordinates of (x, y, z), ($-y$, $x-y$, z), and ($y-x$, $-x$, z). This is with respect to a hexagonal unit cell (shown in Figures 6 and 7) with an origin at the Si T_1 site and with the c axis along the diamond-cubic [111] direction. The projection of the three Br positions into the same primitive unit cell produces a Br triplet, which in this case is laterally centered about the T_4 site. This constitutes a crystallographic measurement of the molecular tilt direction. If, for example, the **Br-Sty** molecules had leaned toward

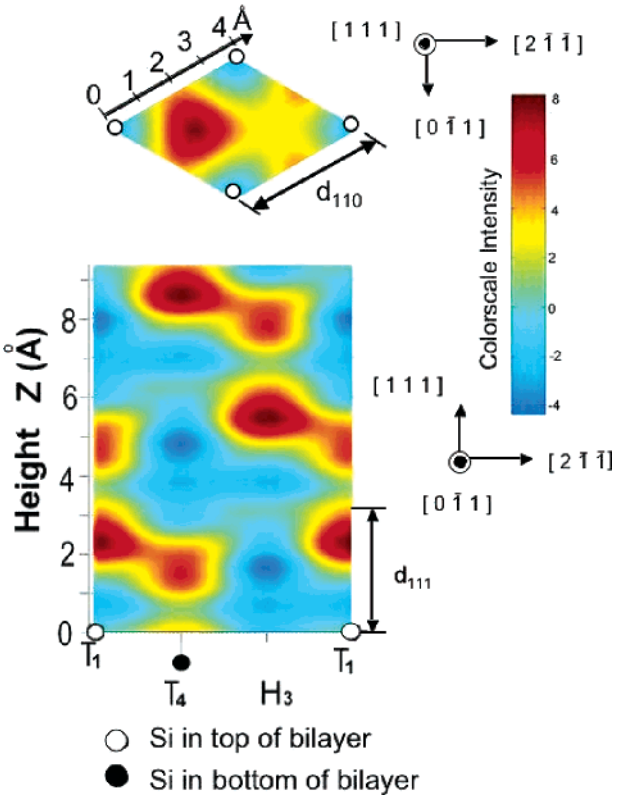

Figure 6. XSW-generated Br atomic map with respect to the Si hexagonal unit cell that exhibits the 3-fold symmetry of the Si-(111)-1 × 1 surface. These 2D cuts through the 3D Br atomic density map coincide with the Br maxima in the 3D map. The upper image is a top-view cut parallel to the (111) surface at a height of $z = 8.50$ Å above the top bulklike Si(111) atomic layer. The lower image is a side-view cut perpendicular to the (111) surface that coincides with the T_1, T_4, and H_3 high-symmetry sites of the Si(111)-1 × 1 surface. For reference, the bulk-like Si positions for the top bilayer of the Si(111) surface are shown as open and filled circles at the bottom of the lower image. The T_1 site is directly above the topmost Si (open circle) in the Si bilayer, and the T_4 site is directly above the bottom Si (filled circle) in the bilayer. The lateral position for the H_3 hollow site is also indicated.

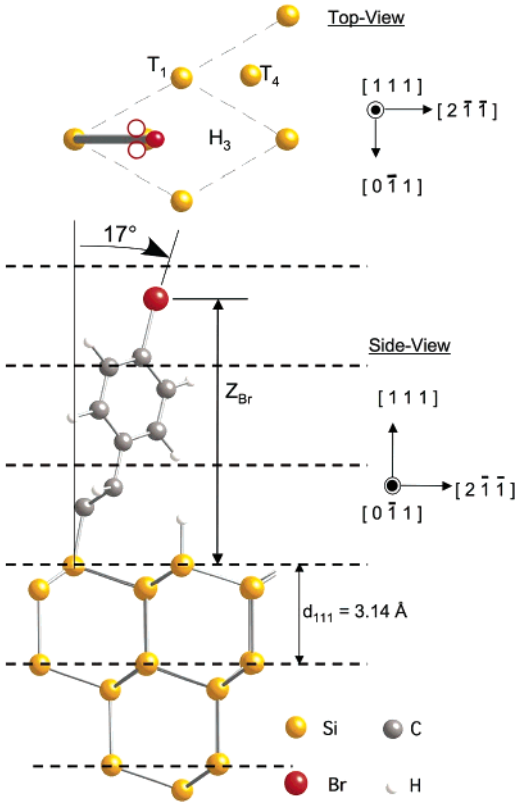

Figure 7. Ball-and-stick model based on the XSW-measured model-independent Br atomic map shown in Figure 6. In the top view of this model, the details of the styrene molecule are replaced with a Br atom tethered to the T_1 Si. The model uses the DFT calculation (Figure 3) to fix the Br−Si molecular length at 8.89 Å and the azimuthal direction of the Si−Br axis to align in the T_1−T_4 direction. The model uses the XRR- and (111) XSW-measured Br height of $z = 8.50$ Å to determine a tilt of 17°. Because of the 3-fold symmetry of the Si(111)-1 × 1 surface, there would be three equally populated configurations that would be ensemble averaged by the XSW measurements. In the top view, all three are shown projected into the same hexagonal unit cell. (The extra two Br atoms are shown as open circles.) The resulting 3-fold-symmetric Br distribution has a maximum density that is laterally centered above the T_4 site.

the H_3 sites (instead of the T_4 sites) to form a film with the same XRR measured electron density profile, then the XSW 3D map would have shown the $z = 8.5$ Å maximum at a H_3 lateral position.

The XSW coherent fraction senses the spread in the Br distribution and can be separated into three factors, namely, $f_H = Ca_HD_H$.[56] For the case of one site along the H direction, the geometrical factor $a_H = 1$. The nonrandom fraction, C, is the fraction of Br atoms located in preferred sites. The Debye−Waller factor $D_H = \exp(-2\pi^2\sigma_H^2/d_H^2)$ treats the time-averaged displacement field of the Br atomic centers as a Gaussian distribution with width σ_H. By assuming $a_{111} = 1$ and by using the measured values of f_{111} and f_{333}, we compute that $C = 0.42$ and $\sigma_{111} = 0.30$ Å for the Br distribution. A similar XSW measurement and analysis was made for the case of 0.5 ML Br directly attached to the Ge(111) surface dangling bond, in which case $\sigma_{111} = 0.08$ Å was reported and was associated with the room-temperature thermal vibrational amplitude of the Br adsorbate.[56] Our presently measured, much larger value of $\sigma_{111} = 0.30$ Å is consistent with Br attached to the surface through a much longer and more complex tether, which would produce height variations in the ensemble of Br atoms. The XSW-measured $\sigma_{111} = 0.30$ Å for Br being smaller than the XRR value of $\sigma_{111} = 1.0$ Å for all atoms in the molecule is consistent because the XSW measurement senses the atomic centers and XRR senses the electron distribution about the centers. This difference can also be attributed to the fact that 58% of the Br atoms are seen by the XSW analysis as being randomly distributed and therefore not included within the $\sigma_{111} = 0.30$ Å Gaussian distribution.

Continuing this type of analysis into the lateral direction by using the measured values for f_{11-1} and f_{220} listed in Table 1, we calculate that $\sigma_{11-1} = 0.74$ Å and $\sigma_{220} = 0.60$ Å for the ensemble-averaged (and time-averaged) Br distribution. The observation that $\sigma_{11-1} > \sigma_{220} > \sigma_{111}$ is consistent with Br atoms attached to an ∼9-Å-long tether that is anchored to the surface with more freedom to have tilt angle changes from molecule to molecule than to have molecular length changes.

4. Conclusions

We have combined a variety of X-ray surface science tools, computational modeling, and scanning probe microscopy to characterize Br-terminated SAMs on Si(111). The XRR and XSW results indicate the formation of a monolayer of thickness 8.5 Å, with the **Br-Sty** molecules tilted at 17° about the [111] axis in the direction of the Si T_4 site and the Br atoms located directly above the Si T_4 sites. The packing density is found to be about

(56) Bedzyk, M. J.; Materlik, G. *Phys. Rev. B* **1985**, *31*, 4110−4112.

0.5 ML. Unlike our earlier report of SAM formation with **Br-UDAME**, which had resulted in the undesired loss of Br atoms to silicon dangling bonds,[32] the present study shows that **Br-Sty** SAMs successfully retain the Br functionality at the top of the organic adlayer. The significance of this result lies in the fact that the Br atoms can now be utilized for further substitutional chemistry to attach a host of other functionalities on top of the SAM.[57,58] In this manner, this work is likely to impact the host of molecular electronic and sensing technologies that have been envisioned for functionalized organic SAMs on silicon surfaces.

(57) Hundertmark, T.; Littke, A. F.; Buchwald, S. L.; Fu, G. C. *Org. Lett.* **2000**, *2*, 1729−1731.
(58) Littke, A. F.; Schwarz, L.; Fu, G. C. *J. Am. Chem. Soc.* **2002**, *124*, 6343−6348.

Acknowledgment. This work was supported by the Nanoscale Science and Engineering Initiative of the National Science Foundation (award numbers EEC-0118025, DMR-0134706, and ECS-0506802), the NASA Institute for Nanoelectronics and Computing (award number NCC 2-1363), and an Office of Naval Research Young Investigator Award (award number N00014-05-1-0563). M.C.H. also acknowledges an Alfred P. Sloan Research Fellowship. The work made use of the Northwestern University Central Facilities supported by the MRSEC program of the NSF (DMR-050513). The XSW measurements were performed at the Advanced Photon Source of Argonne National Laboratory supported by the DOE (W-31-109-Eng-38) using the DuPont-Northwestern-Dow Collaborative Access Team facilities supported in part by the state of Illinois.

LA062759F